

Investigation of Erosive Wear Behavior of Glass-Fiber/Iron-Mud Reinforced Epoxy Hybrid Composite: using Neural Computation and Particle Swarm Optimization

Biswajyoti Pani, Polymersetty Chandrasekhar, Saranjit Singh

School of Mechanical Engineering, KIIT (Deemed to be University), BBSR, Odisha

ABSTRACT

Iron-mining and ore processing are faced with the major challenge of generated overburden and topsoil aggregates as a major solid waste. Storage and reclamation are two severe problems with harmful environmental concerns. The present paper investigates the possible uses of iron mine waste for developing a new-class hybrid polymer composite and its tribological characteristics. The polymer composites are fabricated through a hand-layup process by reinforcement of woven glass fibers in epoxy polymer filled with different weight proportions of iron-mud. Erosion wear experiments were conducted on the fabricated composites according to Box-Behnken experimental design based on Response Surface Methodology approach under controlled laboratory conditions using an air-jet type erosion tester. Artificial Neural Network predicted values exhibited a close relationship with the experimental erosion values. Filler addition resulted in an improvement in the erosion resistance. A metaheuristic approach like particle swarm optimization revealed the minimum erosion value at the optimal parametric combination. Finally, the morphology of eroded surfaces was critically examined by scanning electron microscopy, and the possible erosion mechanisms were presented.

KEYWORDS

Mines waste; polymer composites; erosive wear; morphology; ANN; PSO.

INTRODUCTION

Many technological and industrial engineering applications, for example, load-bearing parts of buildings, tank/vessels, bridges, automobiles applications and so on, considered fiber-reinforced polymer composites (FRPCs) as a feasible option. These FRPCs are widely used as a superior tribo-engineering material given their many advantages like wear resistance and excellent stiffness to weight ratio and strength to weight ratio as compared to monolithic metal alloys. Despite these advantages, its high cost and unstable properties have reduced its use. Fillers that are available in abundance at a low cost are a viable, yet economical, option. The inclusion of fillers has a two-fold purpose: firstly, to add superior mechanical and tribological properties to the component, and secondly, to make the component economical. The investigation of the influence of inclusion of fillers (micrometer-sized particulates) needs necessarily a high filler content of generally 20% to be incorporated into polymer composites. Significant properties, like density, process-ability, aging and appearance may face antagonistic effect due to inclusion of this high filler content[1, 2]. Therefore, the appropriate selection of fillers, fibers, matrix and processing techniques lends itself to the manufacturing of customized materials to meet the needs of specific engineering requirements. Ceramic-filled polymer composites, though extensively researched in the last two decades, are expensive because of the high cost of conventional ceramic fillers. Thus,

exploring the potential of cheap materials like industrial and mines wastes has become important.

India has considerable reserves of moderate to good quality iron ore. The iron ore mining industry employs approximately six million people and generates 2.3% revenues of India's gross domestic product. However, the mining industry in India is facing many problems. For example, in a tiny state like Goa, which is the largest employing mining industry, the major problems are storage issues and reclamation overburden (mine wastes, i.e., overburden and topsoil for accessing the iron ore). Figure 1a shows the waste generated during the processing of the mine and ore. These wastes are made up of minerals related to the ore body and host rock, and sometimes the clay. Various potential adverse effects of mine waste that jeopardize the surrounding environment through siltation/sediment deposition into both agricultural fields (results in poor harvest) and rivers (results in restricted navigation) have been studied. In addition, heavy metals from mine wastes leach into surface and ground waters, resulting in the reduction of both fish populations and the amount and quality of drinking water. The sulfide minerals (pyrrhotite, marcasite, arsenopyrite) known for their potentially acid producing characteristics have also been found in the soils from the iron ore mining areas. The mining companies are beset by the challenge of procuring additional private land (outside the lease area) for removal and disposal to meet the present high ore-overburden at ever-increasing costs. Figure 1b provides a graphical summary of the possible utilization of mine waste. Significant global efforts are being made to explore the implication of mine waste in countries with less land for dumping, for example, France and Germany. A few researchers have studied the utilization of overburden in construction, Linz-Donawitz slag, and iron-ore-tailings as fillers in polymer composites [3-5]. Recently, Pani et al. [6] have reported exhaustively on the abrasion wear behavior of iron mud/glass fiber (GF)-reinforced epoxy composites. The possibility of inclusion of iron-mud in FRPCs that could provide a synergism in terms of enhanced performance like superior erosion wear resistance, yet to be studied, has been examined in this article.

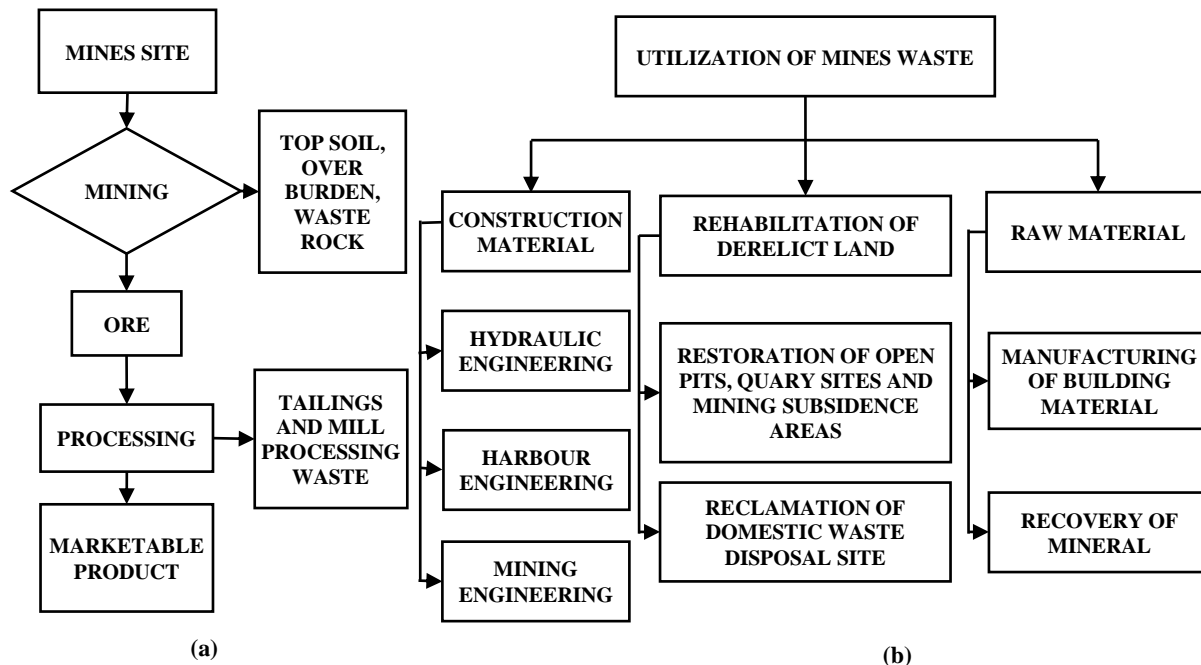


Fig 1: Schematic representation of (a) waste generation in mines and (b) Potential uses

The industries encounter erosion wear for the failure of a significant number of engineering components, out of which some are made from FRPCs [7]. Mechanical and

tribological properties are being examined so that the cost of replacement and material wastage of spares can be lowered. Solid particle erosion (SPE) is the natural wear of the surface of the body due to the mechanical interaction between that solid particulate matter and surface. Damage caused in several industries by erosion, like pipes carrying airborne solids or fly ash-affected boiler tubes and gas turbine blades, plays a critical role in their operational performance in the dusty environment [8-11]. To decrease or control this erosion wear, appropriate selection of materials during design and the complete knowledge of effect variables on the decay rate have become highly essential.

A review of literature emphasized the influence of SPE and identified the enhancement of erosion resistance by using bidirectional woven E-glass fiber. Furthermore, concluded that the erosion wear response of combined fiber and filler along with statistical analysis is comparatively less [12]. Few researchers indicated that fillers like alumina, red mud, SiC, granite, fly ash, copper slag, LD-slag integrated into the polymer matrix, etc. reduce the rate of material loss significantly during erosion [2, 4, 13-17]. However, a recent literature review [18] suggests that the investigation of SPE on polymer composite is not available to the same degree as for ceramics or metals till date and also explored the need for further study to investigate the erosion wear behavior on different types of alloy and composite material as the target material.

This study aims to determine the potentiality of this abundant overburden (mines waste) as particulate filler in polymers so as to develop low cost, lightweight, high strength, and erosion wear-resistant composites. It not only presents a new class of hybrid polymer composites but investigates their tribological performances also. The composites were fabricated using hand-layup process by reinforcing woven GFs in the epoxy polymer filled with different weight proportions of iron-mud. Till date, most of the studies on polymer composites are based on either unidirectional or randomly oriented fibers. Nowadays, woven FRPCs have received increased attention mainly because of the ease of handling during fabrication and balanced properties in the fabric plane. Present research considers bi-directionally woven GF-reinforced polymer composites as they exhibit enhanced wear resistance mainly because of the parallel and perpendicular weaved configuration reinforcement fiber in the composite. Furthermore, GFs are widely available and inexpensive. The erosion wear experiments are performed as per Box-Behnken design approach under controlled laboratory conditions using an air jet-type erosion tester. An artificial neural network (ANN) model was developed for enhanced analysis and prediction of wear behavior and to assess the damage due to wear, with metaheuristic particle swarm optimization (PSO) technique for minimum erosion value at the optimal parametric combination. Scanning electron microscopy (SEM) was used to check the morphology of eroded surfaces, and the possible erosion mechanisms are presented.

MATERIALS AND METHODS

Materials

In the present fabricated composite, the raw material used as the matrix material is Epoxyl-56L (Chemical Name-Bisphenol-A-Diglycidyl-Ether), having an elastic modulus of 3.42 GPa and density of 1.19 gm/cc that can be cured at room temperature. Epoxy was used because of its high rigidity, superior wear and thermal properties, satisfactory corrosion resistance to alkali and acid, and less volumetric shrinkage during curing, exhibiting excellent dimensional stability in electronic and coating industries [6].

E-glass fibers (plain weave, elastic modulus 72.5 GPa, and density 2.59 gm/cc) were used as reinforcement, and iron-mud particles collected from OCL India Ltd., Rajgangpur, Odisha, India, having a size range of 75-150 μ and dried completely in the sunshine and kept in an oven at 100°C, were used as filler material. The density of iron-mud was found to be 2.8

gm/cc. Wet Chemical Analysis on iron mud suggests loss on ignition -9.25%, Fe₂O₃-71.35%, Al₂O₃-9.11%, SiO₂-8.39%, CaO-1.87% and traces of MgO and TiO₂ (0.03%).

Fabrication of composite

Epoxy resin (56L) and its hardener (MH91), made by Marshal Polymer Ltd., were manually mixed by a mechanical stirrer to enhance the dispersion of the filler particulate in the polymer matrix in 10: 1 ratio as per weight recommendation. Unidirectional composite laminates with different weight percentage (0, 5, 10, 15 and 20 wt%) of iron- mud content, with 50% weight fraction of GF (8-layer) were fabricated by conventional hand lay-up process under light compression mold (stainless steel of 250 mm × 250 mm × 3.5 mm dimensions) for proper curing. Load applied during light compression molding was 25 kg for 24 h. The fabricated composites were further cured for 2 h in the hot air-oven at 100°C. To ease the removal of the composite from the mold, silicon spray was used as a releasing agent. Specimens of suitable dimensions were prepared as per ASTM standard using a diamond cutter for further investigations. Table 1 represents the composition of fabricated composites in the present investigation.

Table 1. Composition of the fabricated composites and abbreviations

Sl No	Symbol	Composite Composition		
		Glass Fiber	Epoxy	Iron Mud
1	C1		50%	0
2	C2		45%	5%
3	C3	Maintained at 50%	40%	10%
4	C4		35%	15%
5	C5		30%	20%

Erosion test

The SPE test was conducted as per ASTM G76 [19] on the air-jet type erosion tester (DUCOM TR-470). The test setup contains an accelerating chamber, air compressor, a conveyor belt-type feeder, an air drying unit and mixing chamber. Schematics of erosion testing machine illustrated in figure 2a. The aluminum oxide (Al₂O₃) sand with particle size 50 µm carried into the mixing chamber by conveyor belt feeder where it mixes with the dry and compressed air. While passing through the nozzle (Tungsten Carbide, 1.5 mm internal diameter), sand particles get accelerated. The erodent particles strike the specimen placed at various angles (30, 60, 90°). The velocity of the eroding particle was calculated using the standard double-disc method [16]. The samples were washed with acetone and dried, followed by precise weight measurement using a precision electronic balance of an accuracy of ±0.01 mg. Erosion value (E_v) was calculated from the data of loss in volume per kg of erodent. The method was repeated until the erosion rate achieved a fixed value known as steady-state erosion rate. Table 2 represents the setting parameters for SPE test. The specimens used for SPE test are shown in figure 2b.

Table 2. Configuration parameters for Air-Jet Erosion Test Rig.

Control factors	Fixed parameters	
Erodent Velocity	Erodent	Aluminum Oxide (Al ₂ O ₃) 50 μm
Erodent discharge rate	nozzle (mm)	Tungsten Carbide (1.5φ x 50 mm long)
Impinging angle	Stand-off distance (mm)	10
	Test Condition	Ambient
	Test Duration (min)	5
	Measurement Scale	Make: Sartorius, (Least count: 0.01 mg)
	Sample Size	25x25x3.5 mm

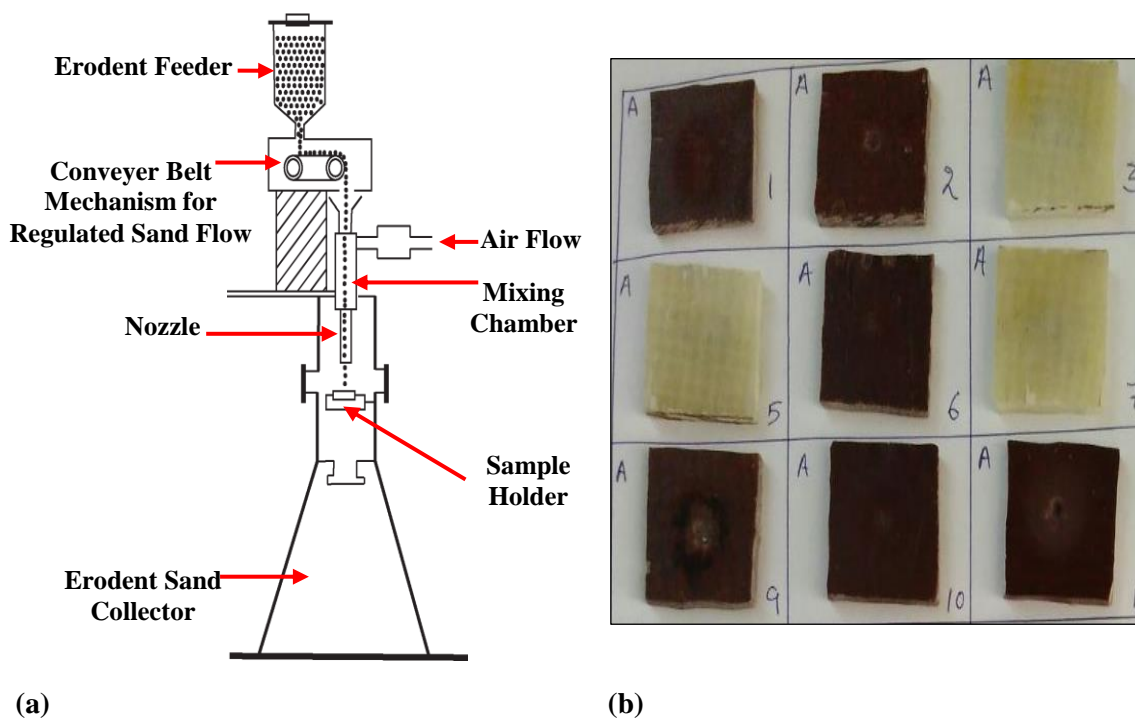


Fig. 2 (a) Schematics of air jet-type erosion testing machine (b) eroded test samples

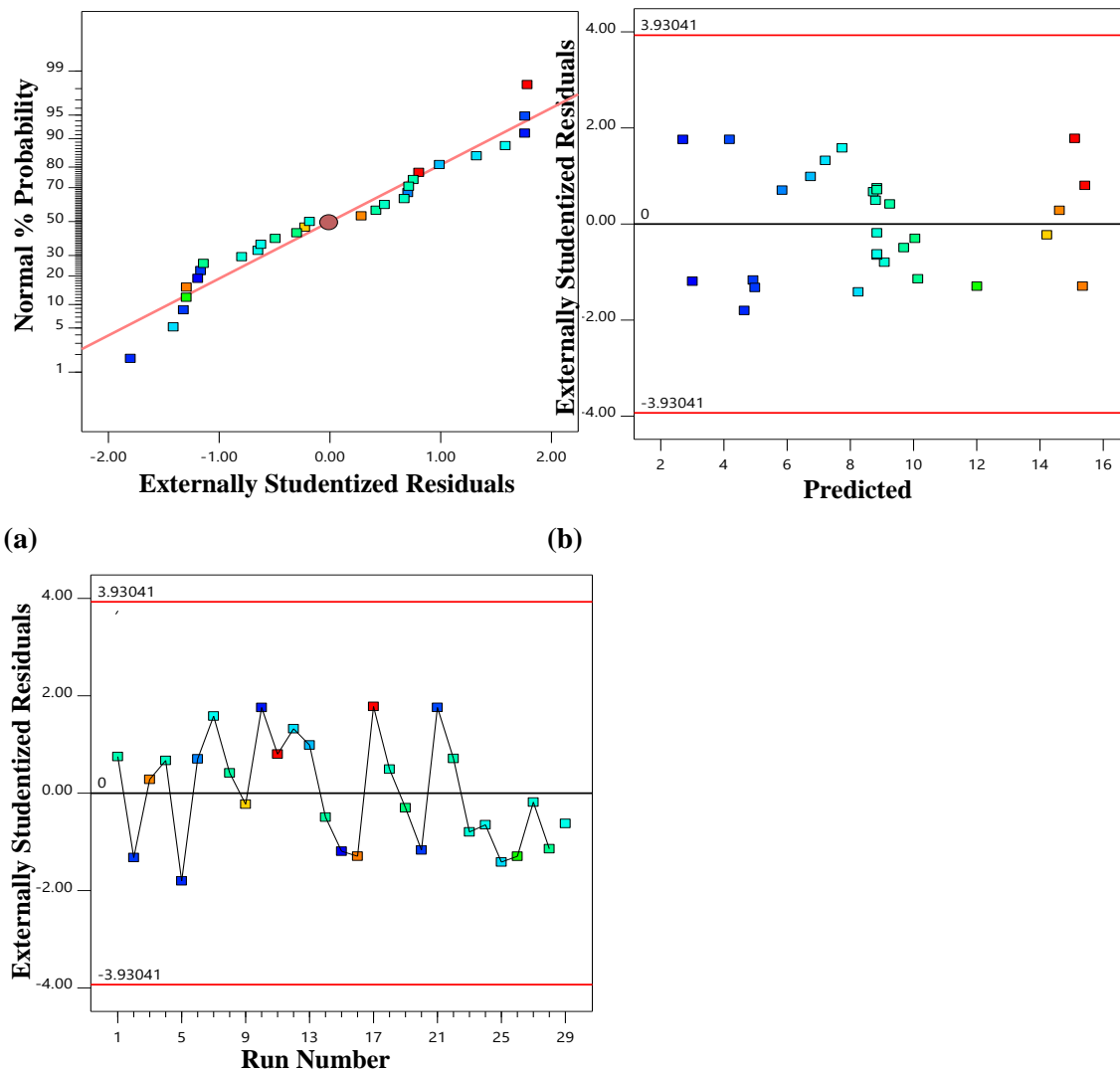
The four-variables randomized Box-Behnken design of experiment (DOE), based on response surface methodology, was adopted to investigate erosion wear characteristics. The present analysis considers four ‘factors,’ e.g., iron-mud content (A), impact velocity (B), impinging angle (C), and erodent mass flow rate (D), and one response variable, i.e., erosion value. The factor levels and their descriptions are shown in Table 3. The Box-Behnken design reduces the number of experimental runs through process optimization. The design was developed using Design Expert® 10.0.3.1 (Stat-ease, Inc. Minneapolis, USA). It included 29 experimental runs and 5 center points as shown in Table 4. Figure 3a-c represents the statistical diagnostics of the data collected through Box-Behnken DOE. Figure 3a indicates residuals are in normal distribution, figure 3b shows no outliers, and figure 3c shows a random scatter and provides guidance against trends that destroy the analysis. Figure 3a-c conclude that data collected from the experiments are safe and reliable for further study.

Table 3. The levels of the factors for Four factor Box-Behnken design

Independent variables	Symbols	Units	Coded and actual levels		
			Low (-1)	Mean (0)	High (1)
Iron-Mud content	A	%	0	10	20
Erodent Velocity	B	m/s	70	110	150
Erodent discharge rate	C	gm/min	4	8	12
Impinging angle	D	degree	30	60	90

Table 4. Design matrix for air-erosion test along with response

Expt.	A	B	C	D	Observed Response	ANN Prediction	Error
	%	m/s	gm/min	degree	(E_v)mm ³ /kg	mm ³ /kg	%
1	10	110	8	60	86.1357	81.78273	5.05
2	10	110	12	90	19.7863	21.75782	9.96
3	0	150	8	60	217.264	197.6155	9.04
4	20	110	12	60	81.2222	87.8511	8.16
5	0	70	8	60	11.6336	10.59126	8.96
6	10	70	4	60	37.6886	41.19267	9.3
7	0	110	12	60	69.9189	69.78263	0.19
8	10	110	4	30	88.8778	88.93577	0.07
9	10	150	12	60	199.468	197.0903	1.19
10	10	70	8	90	11.4354	12.21387	6.81
11	20	150	8	60	248.349	267.8251	7.84
12	20	110	8	90	59.9535	64.9853	8.39
13	0	110	8	90	51.1376	46.42278	9.22
14	20	110	8	30	89.9441	90.25352	0.34
15	10	70	12	60	6.3481	5.72997	9.74
16	10	150	8	30	219.824	206.3748	6.12
17	10	150	4	60	249.187	273.2796	9.67
18	10	110	12	30	81.2011	89.10249	9.73
19	0	110	4	60	98.3804	90.15955	8.36
20	20	70	8	60	19.7787	18.56772	6.12
21	10	70	8	30	23.6079	25.7933	9.26
22	10	110	8	60	85.7198	79.78273	6.93
23	0	110	8	30	76.4794	68.95864	9.83
24	10	110	8	60	71.6257	77.78273	8.6
25	10	110	4	90	59.0588	60.9163	3.15
26	10	150	8	90	131.841	119.7319	9.18
27	10	110	8	60	76.2843	75.78273	0.66
28	20	110	4	60	93.5478	96.5149	3.17
29	10	110	8	60	71.8755	76.78273	6.83

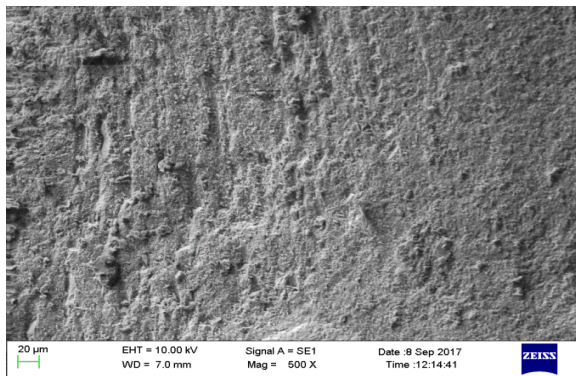


(a) Normal Probability plot (b) Residuals Vs Predicted (c) Residuals Vs Run for erosion wear Scanning electron microscopy

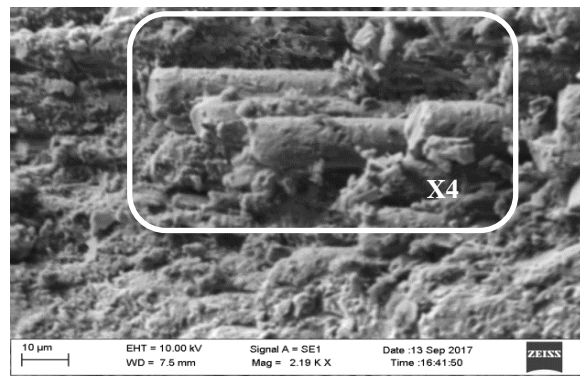
The SEM (EVO MA 15, CARL ZEISS SMT, Germany) was used to examine the surface morphology of the specimens. Gold-palladium was used to sputter coat (thickness - 150 Å) the eroded samples to augment the conductivity. The eroded samples were mounted on stubs with adhesive carbon tape. The morphology of eroded surfaces were presented in figure 4.

Artificial neural network

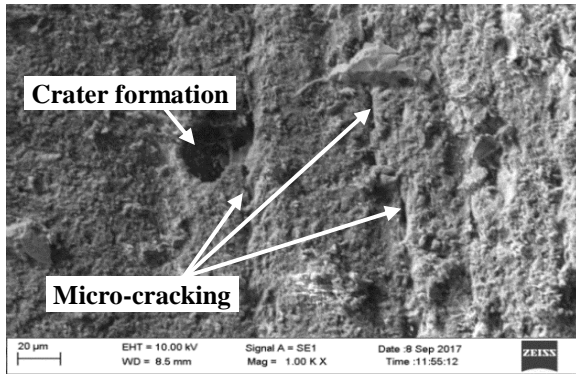
The ANN was implemented to learn and simulate randomly chosen test dataset of 29 independent wear measurements, generated during the erosion trials on the composites using the “Neural Network Toolbox” of MATLAB. A structured ANN (4- [16-4]₂-1) with two hidden layers (sixteen neurons in the tansig layer and four neurons in purelin) along with an automated Bayesian regularization (trainbr) back-propagation algorithm was finally selected with an acceptable predictive quality with the low value of MSE. The algorithm can identify the optimal size of the ANN in its hidden layers. The current investigation considers four ‘inputs,’ e.g., iron-mud content, impact velocity, impinging angle and erodent mass flow rate, and one ‘output,’ i.e., erosion rate, for modeling ANN. Under the present study, 60% of the data (21 sample data) were used for training, 20% of the data (4 sample data) were used for validation, and the remaining 20% of the data (4 sample data) were used for testing. Various ANN structures were tested with different numbers of neurons in the hidden layer and by considering the coefficient of determination (denoted R), the network performance was assessed.



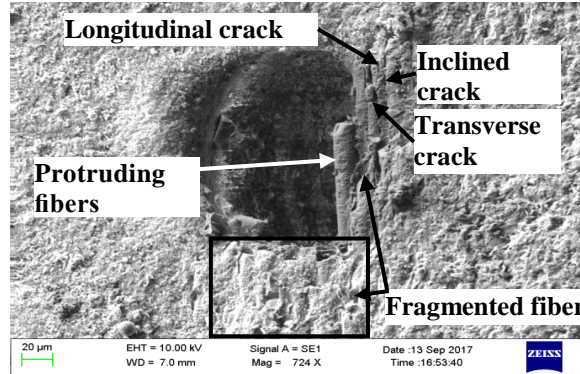
(a)



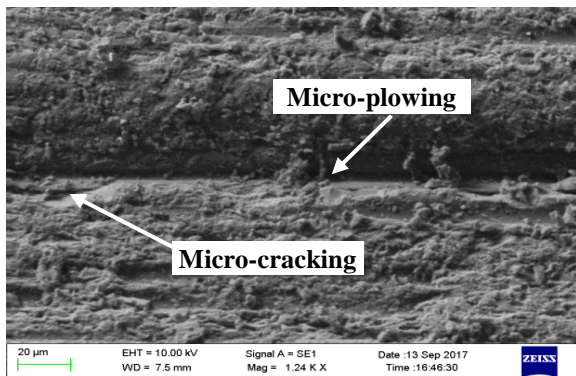
(d)



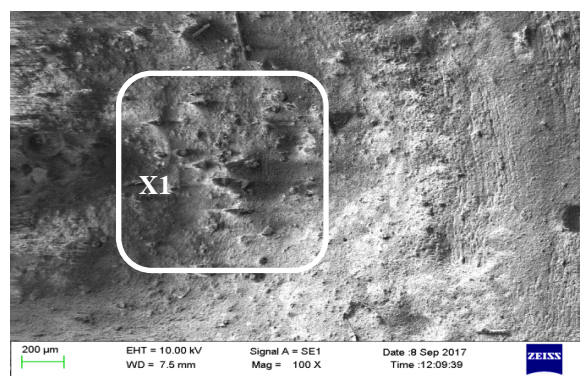
(b)



(e)



(c)



(f)



(g)

Fig. 4 SEM micrographs of the eroded surfaces of C5 at impingement angle of 60° with: (a) – (d) impact velocity of 110 m/s and erodent discharge rate of 12 gm/min; (e) – (g) impact velocity of 150 m/s and erodent discharge rate of 8gm/min

RESULTS AND DISCUSSION

Surface Morphology

The SEM was used to illustrate the morphology of eroded surfaces and identify the mode of material removal of the fabricated composite samples. Figures 4a-g represent the surface microstructures of iron-mud filled GF-epoxy composites. Figures 4a-d show the micro-photographs of the eroded surface of the composite with 20% iron-mud content (C5), at an impingement angle of 60°, impact velocity of 110 m/s and erodent discharge rate of 12 gm/min, whereas, figures 4e-g on the same sample with impact velocity of 150 m/s and erodent discharge rate of 8gm/min.

The surface is roughened due to the repeated impact of these erodent particles as illustrated in figure 4a and this impact is the probable cause for crack initiation and subsequent propagation. These micrographs show features like cracks and craters on the worn surface as shown in figure 4b. The signs of plastic deformation of the matrix material were identified, and when impacted at an angle 60°, the hard erodent particles penetrate the surface and cause material removal, mostly by micro-plowing and micro-cutting as shown in figure 4c. The matrix covering the fiber is chipped off, and the resulting crater reveals the intact fiber body. The wear track is distinctly visible with protruding fibers beneath the matrix layer. The cracks and multiple fractures resulted in fragmentation of the fibers can be distinctly seen. Furthermore, the arrays of broken and semi-broken glass fibers are clearly visible beneath the matrix layer is observed as shown in figure 4e. Figures 4d and f shows fragmented fiber and filler with matrix- micro flake debris (Zone – X1), indicating surface damage due to erosion by aluminum oxide sand particles. Due to the impact of high- velocity erodent particles, multiple grooves of different sizes form (Zone – X2) on the surface are seen in figure 4g. This leads to the removal of material by dislodgement of worn particles from the surface, resulting in the mass loss of the composites.

Wear Analysis and Prediction using ANN

Table 5 represents simulation result of ANN model (all 29 test conditions along with the associated percentage errors along with the experimental erosion value). It seems to establish validation of the ANN model as it exhibits errors within the range of 0–10%. Considering the bigger data sets along with the optimization of the construction of the ANN model, the errors can be reduced further. To quantitatively identify the influence of considered factors on the erosion value and help characterize any polymer composite, the ANN model needs to be well-trained. The generalization behavior of ANN helps us to choose parameters beyond the actual experimental limits. Figure 5a and b represent the possible influence of the significant factors for the erosion value of GF-epoxy hybrid composites (with and without iron-mud).

Effect of impingement angle on erosion wear:

The influence of the impingement angle on the particle erosion has been recognized well by several researchers [12, 18]. The experimental conditions and composition of the target material influence the erosion wear characteristics. Considering the impact of impingement angle on erosion wear characteristics, the possible classification may be in ductile and brittle categories. The peak erosion usually occurring at 15–20° angles comes under ductile erosion behavior, whereas the peak erosion occurring at normal impact, i.e., 90° angles, comes under brittle erosion. The nature of the composite material greatly influences the erosion value at different impact angles [20]. Figure 5a indicates the impingement angle and its effect on the corresponding erosion value of iron mud filled GF-epoxy composites studied from ANN predictive graph. It represents GF-epoxy hybrid composites (with and without iron-mud) exhibiting semi-ductile behavior (neither purely ductile behavior nor purely brittle behavior) to SPE response as maximum erosion occurring at 60°-70° angle of impinging abrasive may be due to the inclusion of GF and iron-mud in the epoxy. Similar observations were reported for GF-epoxy composites containing Al₂O₃, red mud, rice-husk as fillers particles [2, 13, 21].

Effect of impact velocities on erosion wear:

Different impact velocities and their influence on the corresponding erosion value of iron mud filled GF–epoxy composites studied from ANN predictive graph are presented in figure 5b. Interestingly, the graph exhibits exponential behavior. The kinetic energy of the impinging abrasive increases along with an increase in the velocity of the impact and is transferred to the target surface upon impact, leading to a greater loss of material due to erosion. The significant influence of velocity of impact that can dominate the effect of other variables, for example, impingement angle, erodent size, etc., in any erosion test [22] is well understood. Velocity (V) is related to erosion value (E_v) by a power law, given as $E_v = p \times V^q$. Here, p is a material constant, and test conditions, including particle characteristics and the erosion test apparatus, influence the exponent q , which is material independent [23-25].

Erosion efficiency (η):

Primarily, the hardness determines the volume displaced by each impact and not the volume eroded. Thus, it fails to provide sufficient correlation with erosion rate alone. Thus, a parameter called erosion efficiency (η) was proposed to obtain a better relationship that will correlate the volume displaced to the actual volume removed combined with hardness. The primary objective of this parameter is to present the erosion mechanism and determine the efficiency with which the volume eroded to the crater volume by impaction of erodent particle. The erosion efficiency (η_{normal}) for normally impacting a stream of particles (i.e., at $\alpha = 90$) defined by Sundararajan, et al. [20] is given as

$$\eta_{normal} = \frac{2E_r H_v}{\rho V^2} \tag{1}$$

where, E_r - erosion rate (Kg/Kg), H_v - hardness of eroding material (Pa), ρ - density of the eroding material (kg/m^3), and V - velocity of impact (m/s)

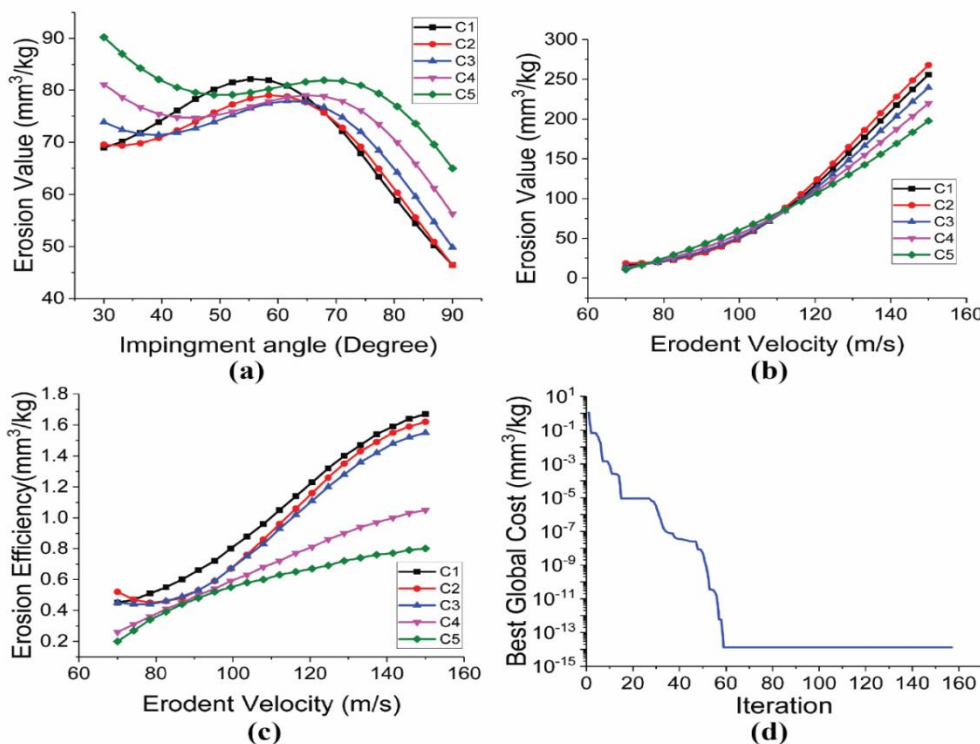


Fig. 5 (a) Impingement angle vs. the erosion value (b) erodent velocity vs. the erosion value (c) erosion efficiency vs. erodent velocity (d) PSO convergence characteristic curve

Table 6 represents the values of erosion efficiencies along with the operating condition of these composites calculated from experimental data using Eq. (1). It demonstrates that

erosion efficiency is not a material property only; however, it somewhat additionally relies upon other operational factors, for example, impingement edge and impact velocity. The estimation of η for a certain impact velocity under oblique impact can be acquired by increasing a factor $1/\sin 2\alpha$ with η_{normal} . Few investigators have previously reported similar observation on velocity dependence of erosion efficiency [16, 26].

The magnitude of η can be utilized to describe the erosion mechanism and its nature. Table 7 represents the erosion mechanism and its nature for different values of erosion efficiency (η) [26, 27]. The erosion efficiencies of the composites under the present study vary from 0.19% to 4.6% for different impact velocities ranging from 70-150 m/s studied. It can, therefore, be concluded that the erosion takes place by micro-plowing and micro-cutting, and semi-ductile composite material exhibits ductile erosion at higher speeds.

Data generated from ANN erosion wear predictive model presented in figure 5c shows that the erosion efficiency of GF epoxy composites with and without iron-mud content increases with an increase in particle velocity. The lower value of erosion efficiencies of composites with 20% iron-mud content (C5) at different impact velocities indicates an excellent erosion resistance, whereas the higher values of erosion efficiencies of GF-epoxy indicate its poor erosion resistance.

Table 6. Erosion efficiency (η) for different iron-mud content

Exp.	A (%)	E_v mm ³ /kg	ρ kg/m ³	B m/s	D degree	Hv Pa	η %
1	10	86.1357	1727.09	110	60	60	1.12
2	10	19.7863	1727.09	110	90	60	0.19
3	0	217.264	1620.92	150	60	35	0.88
4	20	81.2222	1870.70	110	60	52	0.91
5	0	11.6336	1620.92	70	60	35	0.22
6	10	37.6886	1727.09	70	60	60	1.21
7	0	69.9189	1620.92	110	60	35	0.53
8	10	88.8778	1727.09	110	30	60	3.46
9	10	199.468	1727.09	150	60	60	1.39
10	10	11.4354	1727.09	70	90	60	0.27
11	20	248.349	1870.70	150	60	52	1.5
12	20	59.9535	1870.70	110	90	52	0.51
13	0	51.1376	1620.92	110	90	35	0.29
14	20	89.9441	1870.70	110	30	52	3.03
15	10	6.3481	1727.09	70	60	60	0.2
16	10	219.824	1727.09	150	30	60	4.6
17	10	249.187	1727.09	150	60	60	1.74
18	10	81.2011	1727.09	110	30	60	3.16
19	0	98.3804	1620.92	110	60	35	0.74
20	20	19.7787	1870.70	70	60	52	0.55
21	10	23.6079	1727.09	70	30	60	2.27
22	10	85.7198	1727.09	110	60	60	1.11
23	0	76.4794	1620.92	110	30	35	1.74
24	10	71.6257	1727.09	110	60	60	0.93
25	10	59.0588	1727.09	110	90	60	0.57
26	10	131.841	1727.09	150	90	60	0.69
27	10	76.2843	1727.09	110	60	60	0.99
28	20	93.5478	1870.70	110	60	52	1.05
29	10	71.8755	1727.09	110	60	60	0.93

Table 7. The erosion mechanism and its nature for different erosion efficiency (η)

Erosion efficiency (η)	Mechanism	Nature
$\eta = 0$.	Ideal micro-plowing that displaces the material from no erosion the crater without any fracture	
$\eta = 1.0$ or 100%	Ideal micro-cutting.	
$\eta \ll 100\%$	The lip or platelet formation and their fracture result in ductile erosion erosion due to repeated impacts	
$\eta > 100\%$	The spalling and removal of large material chunks in brittle erosion the interlinking of lateral or radial cracks lead to erosion	
$\eta = 10-100\%$	Low impact velocity	semi-ductile
$\eta < 10\%$	Relatively higher impact velocity	ductile erosion

Wear Analysis using Particle Swarm Optimization

Finally, during the present investigations, a nonlinear inertia weight variation for dynamic adaptation-based PSO code was developed and run in the MATLAB interface. It has been observed that heuristics and meta-heuristics techniques are gaining attention due to the failure of traditional regression models in explaining the nonlinear and complex processes in various fields of engineering analysis. PSO is one of the meta-heuristic evolutionary optimization algorithms that generate a population of particles or possible sets of solutions at the end of the each iteration, leading in the direction of optimum value. The rationale behind using the PSO lies in the fact that it can find the globally optimal parameter settings with reduced computational effort and time, whereas the traditional optimization techniques were typically stuck at the local optimum values. Benchmarked standard parameter (acceleration coefficients $c_1, c_2 = 1.0$; Inertia Coefficient $W_{\min} = -0.3, W_{\max} = 0.2$; nonlinear modulation index $n = 1.2$) for nonlinear inertia weight variation for dynamic adaptation-based PSO was used [28]. The iteration was performed, and the PSO convergence characteristic curve is presented in figure 5d. The minimum response predicted from the model is a mean erosion value of $0 \text{ mm}^3/\text{kg}$, and the final optimized wear conditions obtained using PSO are 20% iron-mud content, 70.43 m/s erodent velocity, 10.75 gm/min erodent discharge rate, and 80.24 degrees impingement angle.

Confirmation Experiment

As the last step of modeling, in using the optimal combination level of control factors, it is necessary to make predictions and verify them experimentally. An arbitrary set of factor combination is considered in the present investigation for executing the confirmation experiment. Table 8 represents the comparison of results obtained from the ANN predictive model and results obtained from confirmation experimentation. It indicates the error within 10% for the developed model, which appear to be able to predict the erosion rate to a reasonable accuracy. However, further reduction of errors can be possible by increasing the number of experimental runs. Based on the knowledge of the input parameters, validation of the development of the predictive model for prediction of erosion rate is found satisfactory.

Table 8. Deviation of the predicted and experimental response values

Model	Process Parameters				Response	
	(A)	(B)	(C)	(D)	Erosion Value	Error (%)
Experimental	15	110	8	90	51.94056	---
ANN Predicted					56.27362	8.34

CONCLUSION

Based on the present investigation, the following conclusions are drawn:

- Implementation of ANN for analyzing erosion wear characteristics was successful. Inclusion of iron-mud as a filler improves the erosion resistance behavior for GF-Epoxy hybrid composites significantly. For extreme erosive environments, these GF-Epoxy hybrid composites will be a suitable alternative and can be fabricated by incorporating iron-mud and GF in epoxy. The error associated with experimental results and the predictive model for erosion value is within the range of 0-10%, as presented in the confirmation tests. Conversely, by increasing the number of experimental runs, the error can be reduced further.
- The impingement angle influences the erosion wear of all composites under consideration, exhibiting semi-ductile erosion wear behavior with the maximum wear rate at 60°-70° impingement angle. The erosion efficiency varies from 0.19% to 4.6%, indicating that the erosion wear takes place by micro plowing and micro cutting.
- SEM studies of eroded surfaces support the involved mechanisms for the overall erosion damage of composites. These studies showed plastic deformation, micro-plowing, micro-cracking, exposure of fibers due to the removal of matrix material in the resin area and fiber cracking and removal of the fiber as well as that of material from the fiber-resin interface zones. The resistance of erosive wear improved due to enhanced resistance to the formation of crack growth as a result of iron mud inclusion. The final optimized wear conditions were 20% (iron-mud content), 70.43 m/s (erodent velocity), 10.75 gm/min (erodent discharge rate) and 80.24 degrees (impingement angle), and the resulting erosion value was 0 mm³/kg of erodent as far as the present experimental conditions are concerned.
- The fabricated composites under the current study will find potential application for various components, for example, desert structure, false ceiling, low-cost housing, pipes carrying coals and dust, partition board, industrial fan, and so on. Further, by using other potential fillers, the current investigation can be extended to a new range of hybrid composites.

REFERENCES

- [1] Attwood T, Dawson P, Freeman J, Hoy L, Rose J, and Staniland P. 1981. Synthesis and properties of polyaryletherketones. *Polymer*. 22, 1096-1103.
- [2] Biswas S, and Satapathy A. 2010. A Study on Tribological Behavior of Alumina-Filled Glass-Epoxy Composites Using Taguchi Experimental Design. *Tribol T*. 53, 520-532.
- [3] Yellishetty M, Karpe V, Reddy EH, Subhash KN, and Ranjith PG. 2008. Reuse of iron ore mineral wastes in civil engineering constructions: A case study. *Resour Conserv Recycl*. 52, 1283-1289.
- [4] Pati PR, Satapathy MP, and Satapathy A. 2017. Experimental investigation on Linz-Donawitz slag filled polypropylene composites using teaching-learning based optimization approach. *Polym Compos*. Doi: 10.1002/pc.24434
- [5] Onitiri MA, and Akinlabi ET. 2017. Effects of Particle Size and Particle Loading on the Tensile Properties of Iron-Ore-Tailing-Filled Epoxy and Polypropylene Composites. *Mech Compos Mater*. 52, 817-828.

- [6] Pani B, Chandrasekhar P, and Singh S. 2018. Application of box-behnken design and neural computation for tribo-mechanical performance analysis of iron-mud-filled glass-fiber/epoxy composite and parametric optimization using PSO. *Polym Compos*. Doi: 10.1002/pc.24882.
- [7] Tsuda K, Kubouchi M, Sakai T, Saputra AH, and Mitomo N. 2006. General method for predicting the sand erosion rate of GFRP. *Wear*. 260, 1045-1052
- [8] Wahl H, and Hartenstein F. 1946. Strahlverschleiss. *Frankh'sche Verlagshandlung, Stuttgart*.
- [9] Bitter JGA. 1963. A study of erosion phenomena part II. *Wear*. 6, 169-190.
- [10] Raask E. 1969. Tube erosion by ash impaction. *Wear*. 13, 301-315.
- [11] Hibbert WA, and Roy M. 1965. Helicopter Trials Over Sand and Sea. *J Aero Soc*. 69, 769-776.
- [12] Vigneshwaran S, Uthayakumar M, and Arumugaprabu V. 2017. A review on erosion studies of fiber reinforced polymer composites. *J Reinf Plast Compos*. 36, 1019-1027.
- [13] Biswas S, and Satapathy A. 2009. Tribo-performance analysis of red mud filled glass-epoxy composites using Taguchi experimental design. *Mater Des*. 30, 2841-2853.
- [14] Patnaik A, Satapathy A, Mahapatra SS, and Dash RR. 2008. Implementation of Taguchi Design for Erosion of Fiber-Reinforced Polyester Composite Systems with SiC Filler. *J Reinf Plast Compos*. 27, 1093-1111.
- [15] Rout A, Satapathy A, Mantry S, Sahoo A, and Mohanty T. 2012. Erosion Wear Performance Analysis of Polyester-GF-Granite Hybrid Composites using the Taguchi Method. *Procedia Engineer*. 38, 1863-1882.
- [16] Srivastava VK, and Pawar AG. 2006. Solid particle erosion of glass fibre reinforced flyash filled epoxy resin composites. *Compos Sci Technol*. 66, 3021-3028.
- [17] Biswas S, and Satapathy A. 2010. Use of copper slag in glass-epoxy composites for improved wear resistance. *Waste Manage Res*. 28, 615-625.
- [18] More SR, Bhatt DV, and Menghani JV. 2017. Recent Research Status on Erosion Wear—An Overview. *Mater Today-Proc*. 4, 257-266.
- [19] ASTM G76-13. Standard Test Method for Conducting Erosion Tests by Solid Particle Impingement using Gas Jets. ASTM International. West Conshohocken, PA. (2013).
- [20] Sundararajan G, Roy M, and Venkataraman B. 1990. Erosion efficiency—a new parameter to characterize the dominant erosion micromechanism. *Wear*. 140, 369-381.
- [21] Rout AK, and Satapathy A. 2012. Study on mechanical and tribo-performance of rice-husk filled glass-epoxy hybrid composites. *Materials and Design*. 41, 131-141.
- [22] Lindsley BA, and Marder AR. 1999. The effect of velocity on the solid particle erosion rate of alloys. *Wear*. 225-229, 510-516.
- [23] Chen Q, and Li DY. 2003. Computer simulation of solid particle erosion. *Wear*. 254, 203-210.
- [24] John Rajesh J, Bijwe J, Venkataraman B, and Tewari US. 2004. Effect of impinging velocity on the erosive wear behaviour of polyamides. *Tribol Int*. 37, 219-226.
- [25] López D, Congote JP, Cano JR, Toro A, and Tschiptschin AP. 2005. Effect of particle velocity and impact angle on the corrosion-erosion of AISI 304 and AISI 420 stainless steels. *Wear*. 259, 118-124.
- [26] Arjula S, and Harsha AP. 2006. Study of erosion efficiency of polymers and polymer composites. *Polym Test*. 25, 188-196.
- [27] Roy M, Vishwanathan B, and Sundararajan G. 1994. The solid particle erosion of polymer matrix composites. *Wear*. 171, 149-161.
- [28] Chatterjee A, and Siarry P. 2006. Nonlinear inertia weight variation for dynamic adaptation in particle swarm optimization. *Comput Oper Res*. 33, 859-871